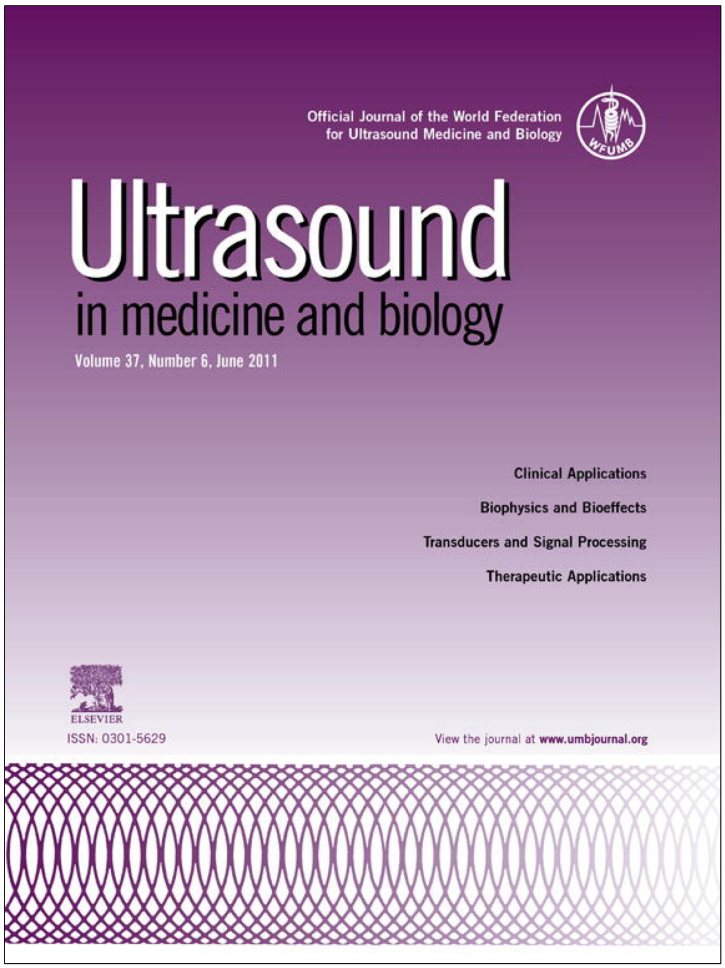

Ultrasound in Med. & Biol., Vol. 37, No. 6, pp. 996–1004, 2011

0301-5629/$ - see front matter

ELSEVIER

doi:10.1016/j.ultrasmedbio.2011.03.009

● *Original Contribution*

# WAVE SIMULATION IN BIOLOGIC MEDIA BASED ON THE KELVIN-VOIGT FRACTIONAL-DERIVATIVE STRESS-STRAIN RELATION

MICHELE CAPUTO,* JOSÉ M. CARCIONE,† and FABIO CAVALLINI†

*Department of Physics, University "La Sapienza", Rome, Italy; and †Istituto Nazionale di Oceanografia e di Geofisica Sperimentale (OGS), Trieste, Italy

(*Received* 20 *December* 2010; *revised* 21 *March* 2011; *in final form* 22 *March* 2011)

**Abstract—The acoustic behavior of biologic media can be described more realistically using a stress-strain relation based on fractional time derivatives of the strain, since the fractional exponent is an additional fitting parameter. We consider a generalization of the Kelvin-Voigt rheology to the case of rational orders of differentiation, the so-called Kelvin-Voigt fractional-derivative (KVFD) constitutive equation, and introduce a novel modeling method to solve the wave equation by means of the Grünwald-Letnikov approximation and the staggered Fourier pseudospectral method to compute the spatial derivatives. The algorithm can handle complex geometries and general material-property variability. We verify the results by comparison with the analytical solution obtained for wave propagation in homogeneous media. Moreover, we illustrate the use of the algorithm by simulation of wave propagation in normal and cancerous breast tissue. (E-mail: jcarcione@inogs.it)** © **2011 World Federation for Ultrasound in Medicine & Biology.**

***Key Words:*** **Biologic media, Anelasticity, Fractional derivatives, Waves, Kelvin-Voigt, Dissipation.**

## INTRODUCTION

The description of the physical and chemical behavior of living matter by using fractional derivatives has recently gained increasing interest in the medical community for the characterization of pathologies. New imaging methods are based on fractional stress-strain relations to interpret data obtained with ultrasound elastography (Coussot et al. 2009), where the shear and Young's moduli are the relevant elastic constants. Fractional derivatives have been used to describe the viscoelastic characterization of liver (Taylor et al. 2002), the flow of small molecules across biologic membranes (Caputo and Cametti 2008a 2008b; Caputo et al. 2009; Cesarone et al. 2005) and breast-tissue attenuation in ultrasound propagation (Bounaïm et al 2007; Bounaïm and Chen 2008). Magin et al. (2009) solved the Bloch equation, which relates a macroscopic model of magnetization to applied radio-frequency in gradient and static magnetic fields, to detect and characterize neurodegenerative, malignant and ischemic diseases. The overview of the methods based on fractional calculus and used in bioengineering is given in Magin (2006).

Stress-strain relations based on fractional derivatives provide a suitable model of wave attenuation in anelastic media. Bland (1960), Caputo (1967), Kjartansson (1979) and Caputo and Mainardi (1971) described the anelastic behavior of general materials over wide frequency ranges by using fractional derivatives, in particular considering propagation with constant-Q characteristics. In this case, Mainardi and Tomirotti (1997) obtained the one-dimensional (1-D) Green's function based on the Mittag-Leffler functions.

One of the most used stress-strain relations for biologic tissues is the Kelvin-Voigt fractional-derivative (KVFD) model, first introduced by Caputo (1981) to model underground nuclear explosions (Taylor et al. 2002; Kiss et al. 2004; Coussot et al. 2009; Kelly and McGough 2009). Since then, several authors studied and used the properties of the KVFD model. Schiessel et al. (1995) obtained analytical solutions in terms of FoxH- and Mittag-Leffer functions. Eldred et al. (1995) fit experimental data for both rubbery and a glassy viscoelastic material. Important applications include biomedical engineering. Zhang et al. (2008) showed that stress relaxation tests on prostate samples produced repeatable results that fit a viscoelastic KVFD model.

Address correspondence to: José M. Carcione, Istituto Nazionale di Oceanografia e di Geofisica Sperimentale (OGS), Borgo Grotta Gigante 42c, 34010 Sgonico, Trieste, Italy. E-mail: jcarcione@inogs.it

Similarly, Coussot et al. (2009) showed that the KVFD relation can characterize the viscoelastic properties of hydropolymers, in particular normal and cancerous breast tissues, stating that this approach may ultimately be applied to tumor differentiation. Here, we consider the KVFD stress-strain relation that is based on three free parameters to describe the viscoelastic behavior of biologic media. Combining this relation with Newton's equation yields the so-called "Caputo wave equation" (Caputo 1967) studied by Holm and Sinkus (2010).

Numerical simulations of wave propagation in an axisymmetric three-dimensional (3-D) domain, based on the Caputo wave equation, have been performed by Wismer (2006) in the low-frequency range, using a finite element method. Regarding other numerical simulations in more than one dimension, Caputo and Carcione (2010) generalized the one-term stress-strain relation (spring or dashpot) to the fractional case, which includes Hooke's law at the lower limit of the fractional order of differentiation and the constitutive relation of a dashpot at the corresponding upper limit. In this case, these authors considered a spectrum of orders of differentiation. The numerical simulation of two-dimensional (2-D) seismic compressional (P)-wave propagation in heterogeneous media for one order of differentiation has been implemented by Carcione et al. (2002), while the 3-D P-S (shear) case has been developed and solved numerically in two dimensions by Carcione (2009). To our knowledge, there are a few works that use the KVFD approach to solve the wave equation in more than one dimension. Besides Wismer (2006), Dikmen (2005) applied the model to simulate 2-D seismic wave attenuation in soil structures and employed the finite-element algorithm to solve the wave equation. In bioacoustics, there is the work of Bounaïm et al (2007) and Bounaïm and Chen (2008), who used a finite-element method to perform 2-D numerical simulations to investigate the detectability of breast tumors. They have used a fractional Laplacian (Chen and Holm 2004) instead of fractional time derivates. It is important to point out that attenuation can also be described by using spatial fractional derivatives (Carcione 2010; Treeby and Cox 2010).

Here, we propose to solve the differential equations with a direct method, where the spatial derivatives are computed by using the staggered Fourier pseudospectral method (*e.g.*, Carcione 2007; Caputo and Carcione 2010). Fractional time derivatives are computed with the Grünwald-Letnikov (GL) approximation (Grünwald 1867; Letnikov 1868; Caputo 1967; Carcione et al. 2002), which is an extension of the standard finite-difference approximation for derivatives of integer order.

In the first part of this work, we introduce the stress-strain relation and calculate the complex moduli, phase velocities and attenuation and quality factors vs. frequency. We then recast the wave equation in the time-domain in terms of fractional derivatives and obtain the GL approximation. The model is discretized on a mesh and the spatial derivatives are calculated with the Fourier method by using the fast Fourier transform. Finally, we perform numerical experiments in breast fatty tissue and breast cancer to study the influence of anelasticity on the wave field. The experiments simulate the clinical amplitude/velocity reconstruction imaging (CARI) technique, which is an ultrasonic method for the detection of breast cancer (Richter 1994). It is based on the reflection of waves at a metallic plate. In CARI, reflection through the breast without the tumor shows a uniform pattern, while in the presence of tumor the field arrives earlier and shows more attenuation.

## MATERIALS AND METHODS

*The stress-strain relation*

Attenuation can be described by means of additional first-order time differential equations (*e.g.*, Carcione et al. 1988; Wojcik et al. 1999) or by using power laws in the form of fractional derivatives. This approach approximates better the behavior of real media. Caputo and Mainardi (1971) describe the anelastic behavior of many materials over wide frequency ranges by using fractional derivatives. We consider the generalization of the Kelvin-Voigt stress ($\sigma$)-strain ($\epsilon$) relation as

$$\sigma = M\epsilon + \eta \frac{\partial^q \epsilon}{\partial t^q}, \quad 0 \leq q \leq 1, \tag{1}$$

where $M$ is the stiffness, and $\eta$ is a pseudo-viscosity, which is a stiffness for q = 0 and a viscosity for q = 1. The limits $q = 0$ and $q = 1$ give Hooke's law and the constitutive relation of a spring in parallel connection with a dashpot, *i.e.*, the Kelvin-Voigt model (Carcione 2007).

In the frequency domain, we obtain

$$\sigma = \overline{M}\varepsilon, \tag{2}$$

where

$$\overline{M} = M + \eta(\mathrm{i}\omega)^q \tag{3}$$

is the complex stiffness, with $\omega$ the angular frequency. We may write (Carcione 2009)

$$\eta = \eta_0 \omega_0^{-q}, \tag{4}$$

where $\omega_0$ is a reference frequency. Then,

$$\overline{M} = M + \eta_0 \left(\frac{\mathrm{i}\omega}{\omega_0}\right)^q. \tag{5}$$

Note that $\eta$ has the units [Pa $s^q$]. The complex modulus $\overline{M}$ given by eqn (5) reduces to the real modulus

$M$ at zero angular frequency; thus, the quasi-static elastic limit is represented by this model.

*Phase velocity, and attenuation and quality factor*

We define the complex velocity as

$$v = \sqrt{\frac{\overline{M}}{\rho}}, \tag{6}$$

where $\rho$ is the mass density. Then, the phase velocity ($v_p$), attenuation factor ($\alpha$) and $Q$ factor are obtained as (Carcione 2007).

$$v_p = \left[\mathrm{Re}\left(v^{-1}\right)\right]^{-1}, \quad \alpha = -\omega \mathrm{Im}\left(v^{-1}\right) \tag{7}$$

and

$$Q = \frac{\mathrm{Re}(v^2)}{\mathrm{Im}(v^2)}, \tag{8}$$

respectively, where "Re" and "Im" denote real and imaginary parts, respectively.

Using eqn (3), we obtain from eqn (6)

$$v^2 = \frac{1}{\rho}[M + \eta\omega^q \exp(\mathrm{i}\theta)] \ , \ \theta = \frac{\pi}{2}q, \tag{9}$$

and

$$Q = \frac{M\eta^{-1}\omega^{-q} + \cos\theta}{\sin\theta}. \tag{10}$$

Equation (9) is equivalent to the dispersion relation of the "Caputo wave equation" studied by Holm and Sinkus (2010) and introduced by Caputo (1967). Holm and Sinkus (2010) show that in the low-frequency range, the attenuation factor $\alpha$ is proportional to $|\omega|^{1+q}$ while at the high frequencies it is proportional to $|\omega|^{1-q/2}$, where the low and high frequencies are determined by the conditions $(\omega\tau)^q << 1$ and $(\omega\tau)^q >> 1$, respectively, where $\tau$ is the relaxation time $\tau = (\eta/M)^{1/q}$.

If $M = 0$, $Q$ is constant (independent of frequency), given by

$$Q = \frac{1}{\tan\theta}, \tag{11}$$

and we obtain the rheology considered by Carcione et al. (2002).

*Two-dimensional dynamical equations*

The conservation of linear momentum for a 2-D linear anelastic medium, describing dilatational deformations, can be written as

$$\rho\partial_t^2 u_i = \partial_i(\sigma + f), \quad i = 1(x), 2(y) \tag{12}$$

(Auld 1990; Carcione 2007), where $u_i$ are the components of the displacement vector, $f$ is the source and $\partial_i$ computes the spatial derivative with respect to $x_i$. The initial conditions are $u_i(0, \mathbf{x}) = 0$, $\partial_t u_i(0, \mathbf{x}) = 0$ and $u_i(t, \mathbf{x}) = 0$, for $t < 0$, where $\mathbf{x}$ is the position vector. The strain-displacement relation is $\epsilon = \partial_1 u_1 + \partial_2 u_2$. Then, the complete set of equations describing the propagation is

$$\begin{aligned} &\partial_t^2 u_1 = \rho^{-1}\partial_1(\sigma + f), \\ &\partial_t^2 u_2 = \rho^{-1}\partial_2(\sigma + f), \\ &\sigma = M\,\epsilon + \eta\frac{\partial^q \epsilon}{\partial t^q}, \\ &\epsilon = \partial_1 u_1 + \partial_2 u_2, \end{aligned} \tag{13}$$

*Numerical algorithm*

The computation of the fractional derivative is based on the Grünwald-Letnikov (GL) approximation (Podlubny 1999; Carcione et al. 2002). The fractional derivative of order $q$ of a function $g$ is

$$\frac{\partial^q g}{\partial t^q} \approx D^q g = \frac{1}{h^q}\sum_{j=0}^{J}(-1)^j \binom{q}{j} g(t - jh), \tag{14}$$

where $h$ is the time step, and $J = t/h - 1$. The derivation of this expression can be found, for instance, in Carcione et al. (2002). The fractional derivative of $g$ at time $t$ depends on all the previous values of $g$. This is the memory property of the fractional derivative, related to field attenuation. The binomial coefficients are negligible for $j$ exceeding an integer $J$. This allows us to truncate the sum at $j = L, L \leq J$, where L is the effective memory length.

Fractional derivatives of order $q << 1$ require large memory resources and computational time, because the decay of the binomial coefficients in eqn (14) is slow (Carcione et al. 2002; Carcione 2009) and the effective memory length $L$ is large. We increase the order of the derivative by applying a time derivative of order $m$ to eqn (13). The result is

$$\begin{aligned} &D^{m+2}u_1 = \rho^{-1}\partial_1\tau, \\ &D^{m+2}u_2 = \rho^{-1}\partial_2\tau, \\ &\tau = MD^m\epsilon + \eta D^{m+q}\epsilon + s, \end{aligned} \tag{15}$$

where we have introduced a causal source term $s = s(t, \mathbf{x}) = D^m f$. It is enough to take $m = 1$ to have a considerable saving in memory storage compared with $m = 0$. In this case, $\tau = \partial_t\sigma$ is the stress rate.

We discretize eqn (15) at $t = nh$ with $m = 1$. Using the notation $u^n = u(nh)$, the left-hand side of the first two equations in (15) can be approximated using

$$h^3 D^3 u_i)^n = u_i^{n+1} - 3u_i^n + 3u_i^{n-1} - u_i^{n-2}, \quad i = 1, 2, \tag{16}$$

where we have used a right-shifted finite-difference expression for the third derivative.

Using eqn (14), the GL derivative in the third equation in (15) can be approximated as

$$D^{m+q}\epsilon \approx \frac{1}{h^{m+q}}\sum_{j=0}^{J}(-1)^j\binom{m+q}{j}\epsilon(t-jh). \qquad (17)$$

Finally, we obtain for $m=1$,

$$\begin{aligned} u_1^{n+1} &= h^3(\rho^{-1}\partial_1\tau^n)+3u_1^n-3u_1^{n-1}+u_1^{n-2},\\ u_2^{n+1} &= h^3(\rho^{-1}\partial_2\tau^n)+3u_2^n-3u_2^{n-1}+u_2^{n-2},\\ \tau^n &= \frac{M}{h}(\epsilon^n-\epsilon^{n-1}) + \frac{\eta}{h^{q+1}}\sum_{j=0}^{J}(-1)^j\binom{q+1}{j}\epsilon^{n-j}+s^n, \end{aligned} \qquad (18)$$

The spatial derivatives are calculated with the staggered Fourier method by using the fast Fourier transform (FFT) (Carcione 1999; Carcione 2007, 2009). The Fourier pseudospectral method has spectral accuracy for band-limited signals. Then, the results are not affected by spatial numerical dispersion. Grid staggering requires averaging the material properties to remove diffractions arising from the discretization of the interfaces. At half-grid points, we average the values defined at regular points. In this case, we apply an arithmetic averaging to the density and the stiffness.

Since we use Fourier basis functions to compute the spatial derivatives, eqn (18) satisfy periodic boundary conditions at the edges of the numerical mesh.

## RESULTS

Analytical solutions of wave propagation problems are exact and conceptually appealing, but can be obtained only under rather restrictive assumptions about the geometry and the nature of the propagation medium. On the other hand, numerical solutions can cope with complex media and arbitrary boundary conditions but are error prone and hence require verification (*i.e.*, tests with synthetic data) and validation (*i.e.*, tests with realistic data).

In this article, we verify our numerical algorithm by comparing numerical and analytical solutions arising from a model that assumes an unbounded homogeneous model. Moreover, we validate it by simulating the CARI experimental technique.

### *Unbounded homogeneous medium*

We consider two breast tissues, specifically, (1) breast fatty tissue and (2) breast cancer, with the following properties: $c_0 = 1475$ m/s, $\eta_0 = 0.01\ M$ and $q = 1.7$ and $c_0 = 1527$ m/s, $\eta_0 = 0.04\ M$ and $q = 1.3$, respectively. These values have been taken from the literature (D'astous and Foster 1986; Weiwad et al. 2000; Bounaïm et al 2007; Bounaïm and Chen 2008). From eqn (9), $M=\rho c_0^2$, where $c_0$ is the velocity at the low-frequency limit. The density for both media is $\rho = 1020$ kg/m$^3$ (ICRU 1998) and the reference frequency is $\omega_0 = (2\ \pi)$ 3 MHz. Figure 1a and b show the phase velocity and quality factor as a function of frequency, where the solid and dashed lines correspond to breast fatty tissue and breast cancer, respectively. It is clear that the second medium is much lossier than the first one.

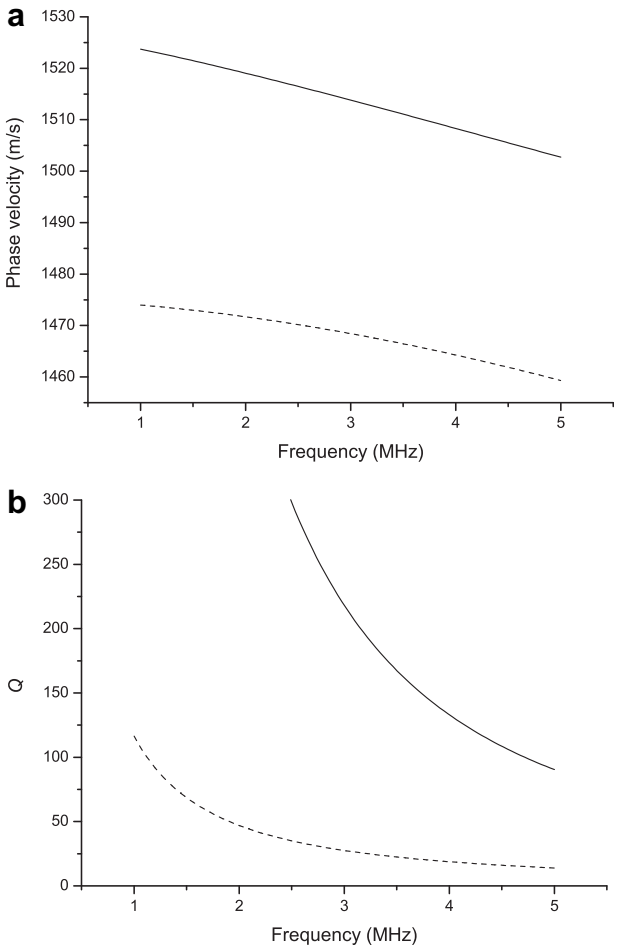


Fig. 1. Phase velocity (a) and quality factor (b) as a function of frequency, where the solid and dashed lines correspond to breast cancer and breast fatty tissue, respectively.

To compute the numerical transient responses, we use the following time-dependence for the source

$$s(t)=\left(a-\frac{1}{2}\right)\exp(-a), \quad a=\left[\frac{\pi(t-t_s)}{t_p}\right]^2, \qquad (19)$$

where $t_p$ is the period of the wave and we take $t_s=1.4t_p$. Its frequency spectrum is

$$S(\omega)=\left(\frac{t_p}{\sqrt{\pi}}\right)\overline{a}\exp(-\overline{a}-\mathrm{i}\omega t_s)\ ,\ \overline{a}=\left(\frac{\omega}{\omega_p}\right)^2,\ \omega_p=\frac{2\pi}{t_p}. \qquad (20)$$

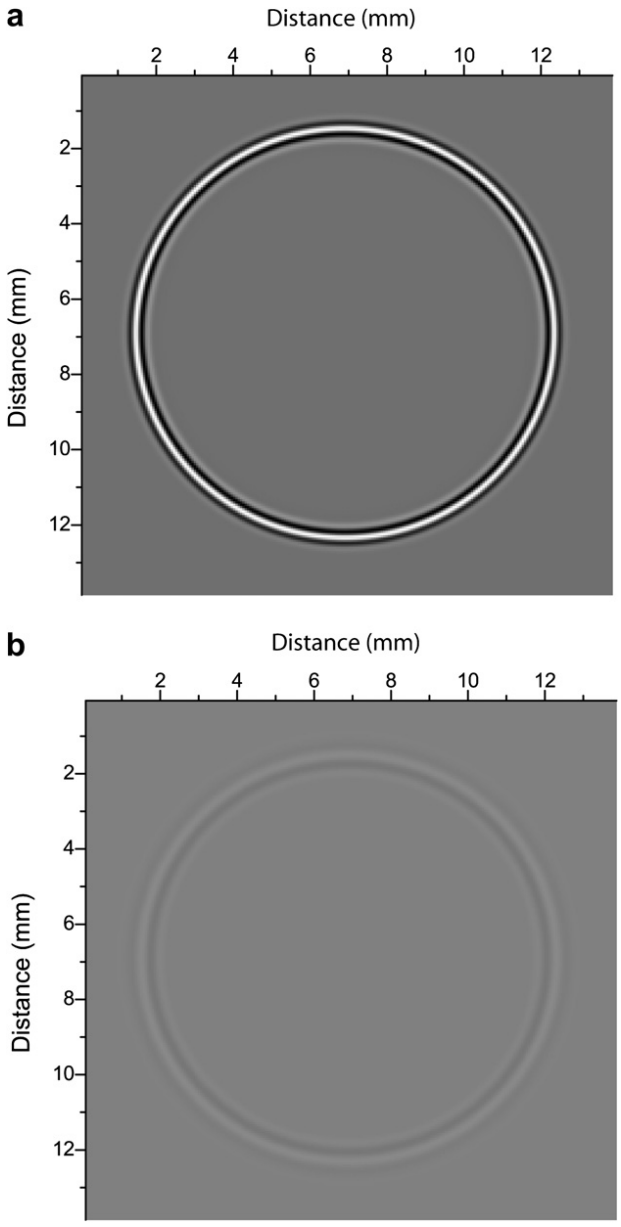


Fig. 2. Snapshots of the dilatational wave in breast cancer tissue at 4 $\mu$s, where (a) corresponds to the lossless medium and (b) to the lossy medium.

The peak frequency is $f_p = 1/t_p$.

We now perform simulations to compare snapshots between a hypothetical lossless medium and the actual medium. A sample of breast cancer is discretized on a numerical mesh, with uniform vertical and horizontal grid spacings of 60 $\mu$m, and 231 $\times$ 231 grid points. A dilatational source is applied at the center of the mesh with a peak frequency of 3 MHz. At this frequency $Q \approx$ 25, according to the dashed line in Figure 1b. We use a memory length $L = 70$ and a time step $h = 5$ ns. Figure 2 shows the snapshots, where the strong attenuation in the real medium is evident (Fig. 2b).

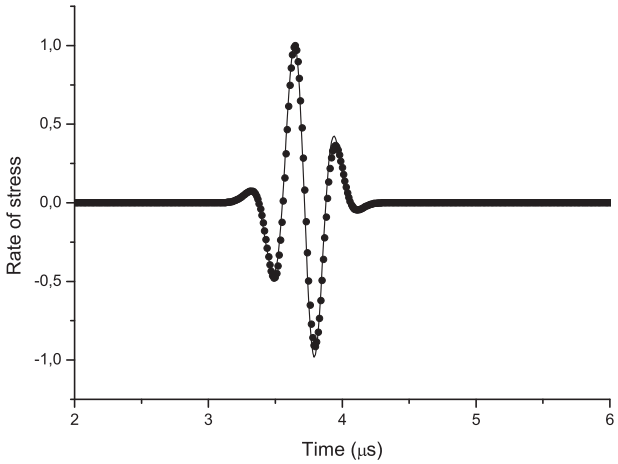


Fig. 3. Comparison between the analytical (solid line) and numerical (dots) solutions at breast cancer tissue. The field is normalized and the source-receiver distance is 4.8 mm.

Figure 3 compares the numerical and analytical transient solutions in breast cancer at a distance of 4.8 mm from the source location. The 2-D analytical solution is obtained in Appendix A. The agreement between solutions has an $L^2$-norm error lesser than 0.5 %.

*Simulation of CARI technique*

The configuration of the CARI technique is shown in Figure 4, where the transducer emits and records the sound field. The metallic plate is made of steel with the

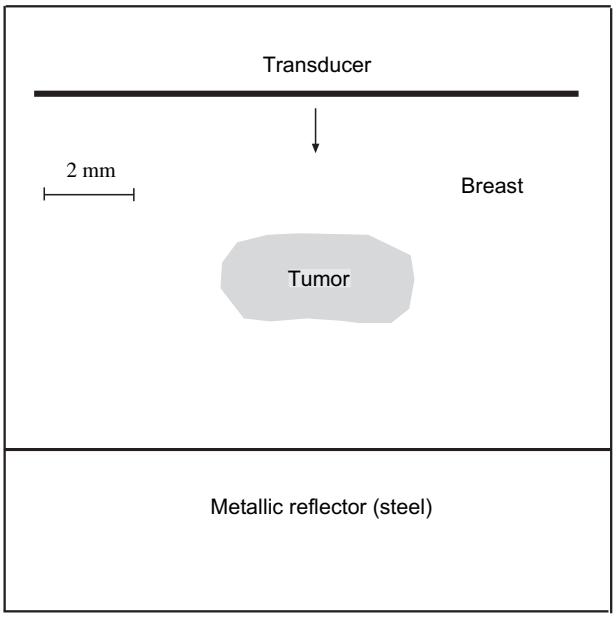


Fig. 4. Two-dimensional model representing the clinical amplitude/velocity reconstruction imaging (CARI) technique for ultrasound breast tumor detection. The transducer is both source and receiver. The wave field is reflected at the metallic plate and returns to the transducer.

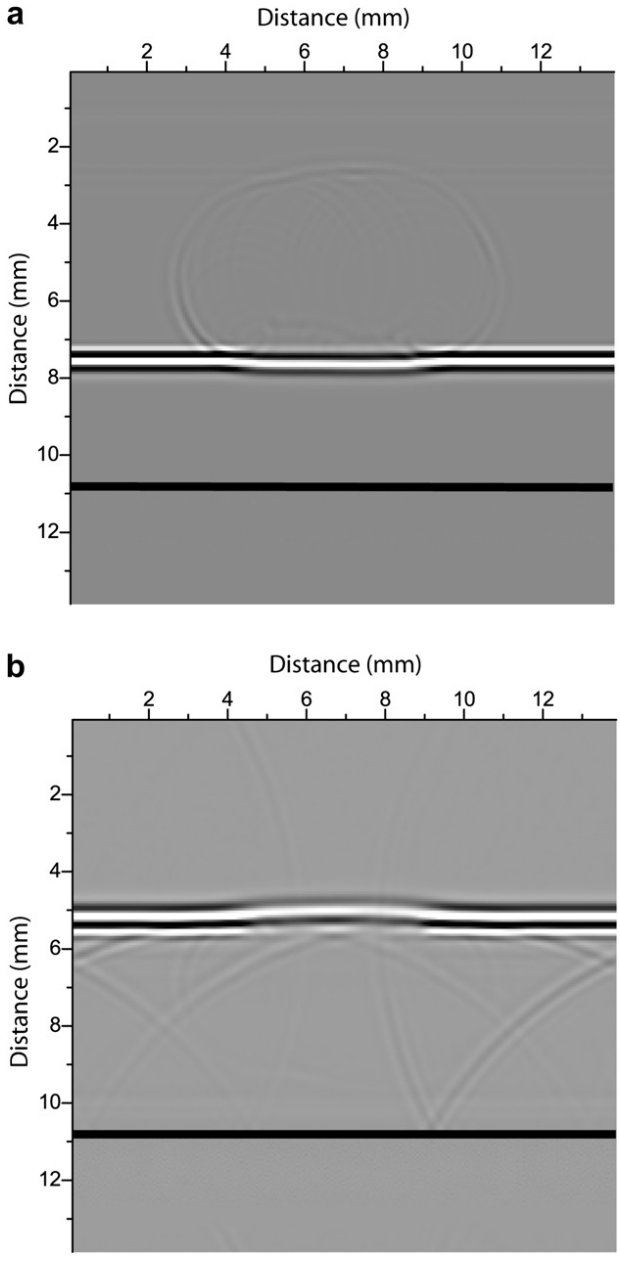


Fig. 5. Snapshots at 4 $\mu$s (a) and 10 $\mu$s (b). The thick line represents the breast/steel interface and the transducer is located at 2.4 mm (vertical distance). A diffraction event arising from the tumor can be seen at 4 $\mu$s.

properties $c_0 = 5900$ m/s, $\rho = 7850$ kg/m$^3$ and no attenuation. The mesh has absorbing boundary conditions at the top and bottom of the grid (20 grid cells) (Cerjan et al. 1985). Due to the periodicity of the Fourier method, the absorbing strip of the top boundary is located at the bottom of the mesh. To be effective, the damping is applied to all the temporal levels, $u^n, n = -2, -1, 0, 1$. We use a memory length $L = 70$ and a time step $h = 2$ ns.

Figure 5 shows snapshots of the wave field at two different propagation times. In Figure 5a, the picture

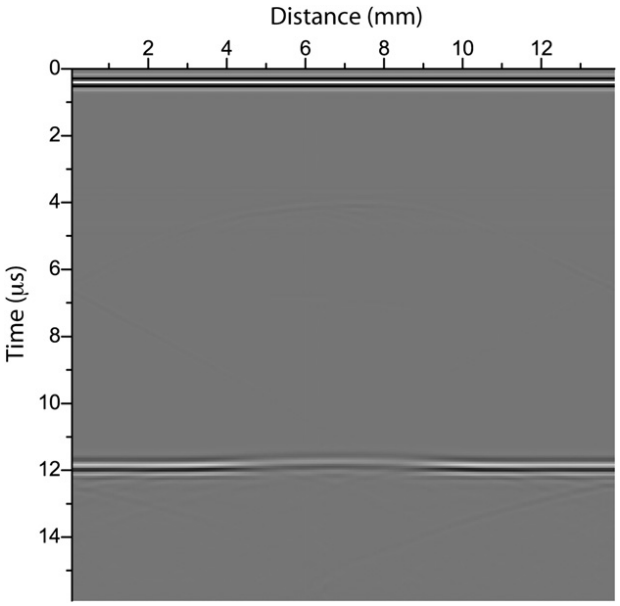


Fig. 6. Time history recorded at the transducer. The reflection event at 12 $\mu$s has a smaller travel time and lower amplitude at the location of the tumor.

shows how the down-going plane wave is diffracted by the tumor, while in Figure 5b the plane wave has been reflected at the breast-steel interface and is traveling back (up) to the transducer line. As can be seen, the field is faster in the region where the tumor is present. The time history recorded at the transducer is represented in Figure 6. The first horizontal event is the initial plane wave, while the reflection event can be seen at nearly 12 $\mu$s, with the signal below the tumor arriving slightly earlier and showing more dissipation.

To show the sensitivity of the technique to the presence of a tumor and attenuation, we represent in Figure 7 the maximum stress rate of the reflection event corresponding to the following cases: (1) without tumor, lossless media; (2) with tumor, lossless media; (3) without tumor, lossy media; and (4) with tumor, lossy media. When there is no tumor the response is flat, while the effect of attenuation is clear in the much lower amplitude of the signal. The simulations show that the CARI technique is suitable for tumor detection.

## DISCUSSION

To our knowledge, the numerical algorithms used to simulate ultrasound in biologic media involving fractional derivatives are based on the finite element (FE) method (Dikmen 2005; Wisman 2003; Bounaïm et al 2007; Bounaïm and Chen 2008). In other fields, the finite difference (FD) method is also used (*e.g.*, Rekanos and Papadopoulos 2010). These algorithms and the Fourier pesudospectral (PS) method have no restrictions on the

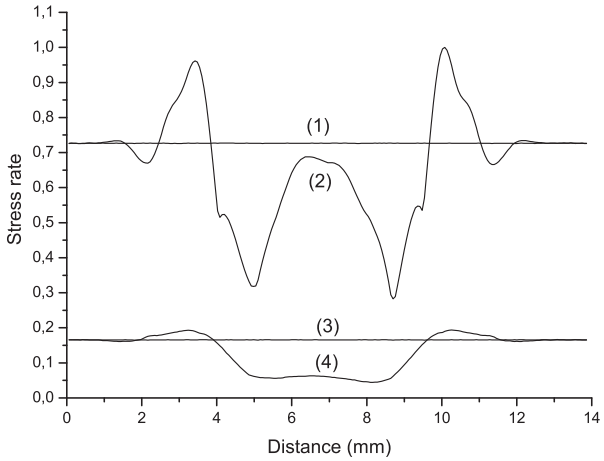


Fig. 7. Maximum stress rate field of the reflection event corresponding to the following cases: without tumor, lossless media (1); with tumor, lossless media (2); without tumor, lossy media (3); and with tumor, lossy media (4).

type of constitutive equation, boundary conditions or source-type and allow general material variability. FD simulations are simple to program and, under not very strict accuracy requirements, are very efficient. Pseudospectral methods can, in some cases, be more expensive, but guarantee high accuracy and relatively lower background noise when staggered differential operators are used. These operators are also suitable when large variations of Poisson's ratio are present in the model (*e.g.*, a fluid-solid interface). On the other hand, FE methods are best suited for engineering problems, where interfaces have well defined geometrical features, in contrast with biologic interfaces. Moreover, use of nonstructured grids, mainly in 3-D space, is one of the main disadvantages of finite-element methods because of the topological problems to be solved when constructing the model.

In particular, the PS method is suitable when the signal propagates long distances. For instance, a 3 MHz signal traveling a distance 10 cm propagates hundred of wavelengths. At these ranges, low-order FE and FD algorithms distort signals unacceptably, while it is known that PS methods are highly accurate (Carcione 2007). In addition, the PS method permits the use of coarse grid sizes. In 3-D space, pseudospectral methods require a minimum of grid points, compared with finite differences and can be the best choice when limited computer storage is available. Fornberg (1996) showed a formal equivalence between the PS method and n-th order FD stencils, where $n$ is the number of grid points. This is the reason for the high accuracy. This property, computational efficiency and parallelism using a large-scale bioacoustic model is illustrated in Wojcik et al. (1999). Optimal performances in geophysics are shown in Carcione et al. (2002) and Carcione (2009).

Another use of the present modeling method could be the simulation of ultrasonic pulse-echo data. Doyle et al. (2010) showed that normal and malignant cells produce time-domain signals and spectral features that are significantly different. The method may have other potential applications in medicine and biology, besides modeling of breast tissue. For example, it could improve the simulation study of contrast microbubbles with a KVFD-type shell instead of the classical KV viscoelastic shell of encapsulation (Chen et al. 2009).

We note that a final test of the method requires a direct comparison of the numerical results with experimental measurements. Also, we should take into account the limitations of the CARI simulations in relation to "realistic" experiments, given the more complex reality of breast cancer assessment with ultrasound (*e.g.*, ductal or lobular carcinoma, natural variations in tissue density and stiffness in normal breast tissue, sources of experimental noise, etc.).

The method can be useful where other techniques may fail, for instance travel time tomography (Schreiman et al. 1984), since the difference in velocity between breast tissue and breast cancer is small.

## CONCLUSIONS

We have presented a numerical algorithm to model ultrasound in biologic tissues based on a generalization of the Kelvin-Voigt model to the case of fractional time derivatives of the strain. This stress-strain relation has three parameters that can be obtained by fitting real data, namely, the stiffness, the pseudo-viscosity and the fractional order. The wave field is computed in the time-space domain using the Grünwald-Letnikov approximation and the staggered Fourier pseudospectral method. The method is successfully tested against an analytical solution and applied to breast cancer detection.

The classical amplitude-velocity reconstruction imaging technique data modeled with the Kelvin-Voigt stress-strain relation, modified with the introduction of fractional derivatives, may possibly indicate the presence of tumor. A further analysis of the physical properties of various tumors and more detailed data are required. Then, the method may lead to the possibility to distinguish between malignant and nonmalignant tumors.

*Acknowledgments*—The authors thank two anonymous reviewers and the editor for useful and detailed comments.

## REFERENCES

Auld BA. Acoustic fields and waves in solids, Vol. 1. Malabar: Robert E. Krieger, Publishing Co.; 1990.

Bland DR. The theory of linear viscoelasticity. Oxford: Pergamon Press; 1960.

Bounaïm A, Holm S, Chen W, Ødegård A. Detectability of breast lesions with CARI ultrasonography using a bioacoustic computational approach. Comput Math Appl 2007;54:96–106.

Bounaïm A, Chen W. Computations for a breast ultrasonic imaging technique and finite element approach for a fractional derivative modeling the breast tissue acoustic attenuation. Int J Tomogr Stat 2008;10:31–43.

Caputo M. Linear models of dissipation whose Q is almost frequency independent-II. Geophys J Royal Astronomic Soc 1967;3:529–539.

Caputo M. Elastic radiation from a source in a medium with an almost frequency independent. J Phys Earth 1981;29:487–497.

Caputo M, Cametti C. Memory diffusion in two cases of biological interest. Theor Biol 2008;254:697–703.

Caputo M, Cametti C. The memory formalism in the diffusion of drugs through skin membrane. Physica D 2009;42:125505–125511.

Caputo M, Cametti C, Ruggiero V. Time and spatial concentration profile of glucose inside an eritrocyte membrane by means of a memory formalism. Physica A 2008;387:210–218.

Caputo M, Carcione JM. Wave simulation in dissipative media described by distributed-order fractional time derivatives. J Vibration Control 2010, in press. [Epub ahead of print].

Caputo M, Mainardi F. A new dissipation model based on memory mechanism. Pure Appl Geophys 1971;91:134–147.

Carcione JM. Staggered mesh for the anisotropic and viscoelastic wave equation. Geophysics 1999;64:1863–1866.

Carcione JM. Wave fields in real media. Theory and numerical simulation of wave propagation in anisotropic, anelastic, porous and electromagnetic media, Amsterdam: Elsevier Science, (Second edition, revised and extended) 2007.

Carcione JM. Theory and modeling of constant-Q P- and S-waves using fractional time derivatives. Geophysics 2009;74:T1–T11.

Carcione JM. A generalization of the Fourier pseudospectral method. Geophysics 2010;75:53–56.

Carcione JM, Cavallini F, Mainardi F, Hanyga A. Time-domain seismic modeling of constant Q-wave propagation using fractional derivative. Pure Appl Geophys 2002;159:1719–1736.

Carcione JM, Kosloff D, Kosloff R. Viscoacoustic wave propagation simulation in the earth. Geophysics 1988;53:769–777.

Cerjan C, Kosloff D, Kosloff R, Reshef M. A nonreflectng boundary condition for discrete acoustic and elastic wave equations. Geophysics 1985;50:705–708.

Cesarone F, Caputo M, Cametti C. Memory formalism in the passive diffusion across a biological membrane. J Membrane Sci 2005; 250:79–84.

Chen W, Holm S. Fractional Laplacian time-space models for linear and nonlinear lossy media exhibiting arbitrary frequency power-law dependency. J Acoust Soc Am 2004;115:1424–1430.

Chen J, Hunter KS, Shandas R. Wave scattering from encapsulated microbubbles subject to high-frequency ultrasound: Contribution of higher-order scattering modes. J Acoust Soc Am 2009;126: 1766–1775.

Coussot C, Kalyanam S, Yapp R, Insana MF. Fractional derivative models for ultrasonic characterization of polymer and breast tissue viscoelasticity. IEEE Trans Ultrason Ferroelectr Freq Control 2009;56:715–726.

D'astous FT, Foster FS. Frequency dependence of ultrasound attenuation and backscatter in breast tissue. Ultrasound Med Biol 1986; 12:795–808.

Dikmen Ü. Modeling of seismic wave attenuation in soil structures using fractional derivative scheme. J Balkan Geophys Soc 2005;8: 175–188.

Doyle TE, Goodrich JB, Ambrose BJ, Patel H, Kwon S, Pearson LH. Ultrasonic differentiation of normal versus malignant breast epithelial cells in monolayer cultures. J Acoust Soc Am 2010;128: EL229–EL235.

Eldred LB, Baker WP, Palazotto AN. Kelvin-Voigt vs. fractional derivative model as constitutive relations for viscoelastic materials. AIAA J 1995;33:547–550.

Fornberg B. A practical guide to pseudospectral methods. Cambridge: Cambridge University Press; 1996.

Grünwald AK. Über "begrenzte" Derivationen und deren Anwendung. Zeitschrift für Angewandte Mathematik und Physik 1867;12:441–480.

Holm S, Sinkus RA. Unifying fractional wave equation for compressional and shear waves. J Acoust Soc Am 2010;127:542–548.

ICRU. Conversion coefficients for use in radiological protection against external radiation. Report 1998;57. Bethesda: ICRU Publications, 1998.

Kelly JF, McGough RJ. Two fractal ladder models and power law wave equations. J. Acoust Soc Am 2009;126:2072–2081.

Kiss MZ, Varghese T, Hall TJ. Viscoelastic characterization of in vitro canine tissue. Phys Med Biol 2004;49:4207–4218.

Kjartansson E. Constant Q-wave propagation and attenuation. J Geophys Res 1979;84:4737–4748.

Letnikov AV. Theory of differentiation of fractional order. Matematiceskij Sbornik 1868;3:1–68 (in Russian).

Magin R. Fractional calculus in bioengineering. Chicago, IL: University of Illinois at Chicago Press; 2006.

Magin R, Feng X, Baleanu D. Solving the fractional order Bloch equation. Concepts Magn Reson 2009;34A:16–23.

Mainardi F, Tomirotti M. Seismic pulse propagation with constant Q and stable probability distributions. Annali di Geofisica 1997;40: 1311–1328.

Podlubny I. Fractional differential equations. San Diego: Academic Press; 1999.

Rekanos IT, Papadopoulos TG. FDTD modeling of wave propagation in Cole-Cole media with multiple relaxation times. Antennas Wireless Propagation Lett IEEE 2010;9:67–69.

Richter K. Technique for detecting and evaluating breast lesions. J. Ultrasound Med 1994;13:782–797.

Schiessel H, Metzler R, Blumen A, Nonnenmacher TF. Generalized viscoelastic models: Their fractional equations with solutions. J Phys A Math Gen 1995;28:6567–6584.

Schreiman JS, Gisvold J, Greenleaf JF, Bahn RC. Ultrasound transmission computed tomography of the breast. Radiology 1984;150: 523–530.

Taylor LS, Lerner AL, Rubens DJ, Parker KJ. A Kelvin-Voight fractional derivative model for viscoelastic characterization of liver tissue. Adv Bioeng 2002;53:1–2.

Treeby BE, Cox BT. Modeling power law absorption and dispersion for acoustic propagation using the fractional Laplacian. J Acoust Soc Am 2010;127:2741–2748.

Weiwad W, Heinig A, Goetz L, Hartmann H, Lampe D, Buchmann J, Millner R, Spielmann RP, Heywang- Kbrunner SH. Direct measurement of sound velocity in various specimens of breast tissue. Invest Radiol 2000;35:721–726.

Wismer MG. Finite element analysis of broadband acoustic pulses through inhomogenous media with power law attenuation. J Acoust Soc Am 2006;120:3493–3502.

Wojcik G, Mould J, Carcione LM, Ostromogilsky M, Vaughan D. Combined transducer and nonlinear tissue propagation simulations. ASME International Mechanical Engineering Congress and Exposition. November 14-19, 1999, Nashville, TN, USA.

Zhang M, Nigwekar P, Castaneda B, Hoyt K, Joseph JV, di Sant'Agnese A, Messing EM, Strang JG, Rubens DJ, Parker KJ. Quantitative characterization of viscoelastic properties of human prostate correlated with histology. Ultrasound Med Biol 2008;34: 1033–1042.

## APPENDIX A

## GREEN'S FUNCTION AND ANALYTICAL SOLUTION

A 2-D analytical solution corresponding to eqn (15) with $m = 1$ in a homogeneous medium can easily be obtained. Combining the equations, we have

$$\partial_t^3 \epsilon = \frac{1}{\rho} \Delta \tau. \tag{21}$$

In the frequency domain, $\sigma = \overline{M}\epsilon$, according to eqn (2), and using (15), eqn (21) becomes a Helmholtz equation,

$$\Delta\epsilon + p^2\epsilon = -\frac{1}{\mathrm{i}\omega\rho v^2}\Delta s = -\frac{1}{\mathrm{i}\omega\overline{M}}\Delta s, \;\; p = \frac{\omega}{v}, \tag{22}$$

where $p$ is the wave number and $v$ is given by eqn (6). If $v$ is real, the medium is lossless. The solution to the acoustic (lossless) equation $(\Delta + p^2)G = -8\delta(r)$ is the Green function $G = -2\mathrm{i}H_0^{(2)}(pr)$, with $v = c_0$, where $H_0^{(2)}$ is the zero-order Hankel function of the second kind (*e.g.*, Carcione, 2007). More precisely,

$$G(x, y, x_0, y_0, \omega, c_0) = -2\mathrm{i}H_0^{(2)}\left(\frac{\omega r}{c_0}\right) \tag{23}$$

where $(x_0, y_0)$ is the source location, and

$$r = \sqrt{(x - x_0)^2 + (y - y_0)^2}. \tag{24}$$

The anelastic solution is obtained by invoking the correspondence principle (Bland 1960), *i.e.*, by substituting the acoustic velocity $c_0$ with the complex velocity $v$. The differential operator $\Delta/(\mathrm{i}\omega\overline{M})$ acts on the source in eqn (22). Thus, the Green's function for the strain is

$$G_\epsilon = \frac{1}{\mathrm{i}\omega\overline{M}}\Delta G. \tag{25}$$

Since $\Delta G = -p^2 G$ away from the source and $\sigma = \overline{M}\epsilon$, the Green's function for the stress is

$$G_\sigma = \overline{M}G_\epsilon = -\frac{p^2 G}{\mathrm{i}\omega}. \tag{26}$$

We set $G(-\omega) = G^*(\omega)$, where the superscript * denotes complex conjugation. This equation ensures that the inverse Fourier transform of the Green's function is real. The frequency-domain solution is then given by $\sigma(\omega) = \frac{1}{8}G_\sigma(\omega)F(\omega)$, where $F$ is the Fourier transform of the source time history. Since we are solving the dynamical equation with $m = 1$, our solution is not $\sigma$ but the stress rate $\tau = \partial_t\sigma$. Hence,

$$\tau(x, y, x_0, y_0, \omega) = \frac{1}{8}\mathrm{i}\omega G_\sigma F = -\frac{1}{8}p^2 G_j(x, y, x_0, y_0, \omega, v)F(\omega), \tag{27}$$

Because the Hankel function has a singularity at $\omega = 0$, we assume $G = 0$ for $\omega = 0$, an approximation that does not have a significant effect on the solution (note, moreover, that $F(0) = 0$). The time-domain solution $\tau(t)$ is obtained by a discrete inverse Fourier transform. We have tacitly assumed that $\tau$ and $\mathrm{d}\tau/\mathrm{d}t$ are zero at time $t = 0$.